Nuclear spin conversion of water inside fullerene cages detected by low-temperature nuclear magnetic resonance

Salvatore Mamone, Maria Concistrè, Elisa Carignani, Benno Meier, Andrea Krachmalnicoff, Ole G. Johannessen, Xuegong Lei, Yongjun Li, Mark Denning, Marina Carravetta, Kelvin Goh, Anthony J. Horsewill, Richard J. Whitby, and Malcolm H. Levitt

Citation: The Journal of Chemical Physics **140**, 194306 (2014); doi: 10.1063/1.4873343
View online: http://dx.doi.org/10.1063/1.4873343
View Table of Contents: http://scitation.aip.org/content/aip/journal/jcp/140/19?ver=pdfcov
Published by the AIP Publishing

Nuclear spin conversion of water inside fullerene cages detected by low-temperature nuclear magnetic resonance

Salvatore Mamone,[1,a)] Maria Concistrè,[1] Elisa Carignani,[1] Benno Meier,[1] Andrea Krachmalnicoff,[1] Ole G. Johannessen,[1] Xuegong Lei,[2] Yongjun Li,[2] Mark Denning,[1] Marina Carravetta,[1] Kelvin Goh,[3] Anthony J. Horsewill,[3] Richard J. Whitby,[1] and Malcolm H. Levitt[1,b)]

[1]*School of Chemistry, University of Southampton, Southampton SO17 1BJ, United Kingdom*
[2]*Department of Chemistry, Columbia University, New York, New York 10027, USA*
[3]*School of Physics and Astronomy, University of Nottingham, Nottingham NG7 2RD, United Kingdom*

(Received 20 February 2014; accepted 25 March 2014; published online 20 May 2014)

The water-endofullerene $H_2O@C_{60}$ provides a unique chemical system in which freely rotating water molecules are confined inside homogeneous and symmetrical carbon cages. The spin conversion between the *ortho* and *para* species of the endohedral H_2O was studied in the solid phase by low-temperature nuclear magnetic resonance. The experimental data are consistent with a second-order kinetics, indicating a bimolecular spin conversion process. Numerical simulations suggest the simultaneous presence of a spin diffusion process allowing neighbouring *ortho* and *para* molecules to exchange their angular momenta. Cross-polarization experiments found no evidence that the spin conversion of the endohedral H_2O molecules is catalysed by ^{13}C nuclei present in the cages.
 [http://dx.doi.org/10.1063/1.4873343]

I. INTRODUCTION

Small molecules with sufficient symmetry display the phenomenon of *spin isomerism*, in which the nuclear spin states and the spatial quantum states are entangled as a consequence of the Pauli principle. The seminal case is that of H_2, where the nuclear spin singlet state ($I = 0$) correlates with even rotational quantum numbers J (*para*-H_2), while the nuclear spin triplet states ($I = 1$) correlate with odd values of J (*ortho*-H_2).[1] Spin isomerism is also exhibited by many other small symmetrical molecules, such as water,[2–14] ethene,[15–17] and methane,[18–21] as well as freely rotating parts of a molecule, such as methyl (-CH_3) groups with low rotational barriers.[22–25] In many cases, the process of spin-isomer conversion, which requires a change in nuclear spin symmetry, is considerably slower than the spatial and nuclear spin transitions between quantum states of the same spin isomer. In extreme cases such as *ortho*- and *para*-H_2, the spin conversion process is so slow that the spin isomers behave as separate substances with different physical and chemical properties.[1]

Spin isomerism is linked to important phenomena in nuclear magnetic resonance (NMR). If a compound is enriched in a spin isomer, and reacted chemically, the reaction products may display enormous transient enhancements in the nuclear magnetic resonance signals.[26] In the case of *para*-enriched H_2, this effect is the basis of *para*-hydrogen induced polarization (PHIP) methods.[27–30] The phenomenon of spin isomerism is closely related to that of long-lived nuclear spin states (LLS), which are correlated states of nuclear spins with extended relaxation times, sometimes exceeding the conventional T_1 relaxation time of nuclear magnetization by more than an order of magnitude, and which may be used for a variety of purposes in NMR spectroscopy.[31–39]

The common isotopolog of water (H_2O) displays spin isomerism, with a correlation between the total nuclear spin I and the rotational state designation $J_{K_aK_c}$. *Ortho*-water has total nuclear spin $I = 1$ and odd parity for $K_a + K_c$ in the ground vibrational state. *Para*-water has total nuclear spin $I = 0$ and even parity for $K_a + K_c$ in the ground vibrational state.[2] The energy splitting between the lowest *para*-water and *ortho*-water levels is ∼2.95 meV in the gas phase.[13]

An understanding of water spin isomers and their interconversion is relevant for several reasons. In astrophysics, the ratio of *ortho* and *para*-water is used to estimate the temperature of comets and other interstellar objects.[3–6] There are speculations that bulk *para*-enriched H_2O might be used to enhance NMR and magnetic resonance imaging (MRI) experiments.[7,8] Unfortunately, the spin conversion of water has proved difficult to study in the condensed phase. The bulk enrichment of water spin isomers through the selective absorption of water vapor on charcoal[8] has been claimed, although the observation is contested.[9] Small quantities of *ortho* and *para*-water have been separated in molecular beams in the presence of a magnetic field gradient.[7]

Proton exchange and intermolecular interactions between neighbouring water molecules may be inhibited by isolating the water molecules. One approach is to dilute the molecules in a frozen inert gas or *para*-hydrogen matrix.[10–12] However, this approach only permits study at low temperature, does not eliminate the formation of dimers and clusters, and does not in general provide a homogeneous and controlled environment for the water molecules. A convenient alternative, which is used in this paper, is to isolate the water molecules by trapping them inside fullerenes (C_{60}) cages, in the form of the

a)s.mamone@soton.ac.uk
b)mhl@soton.ac.uk

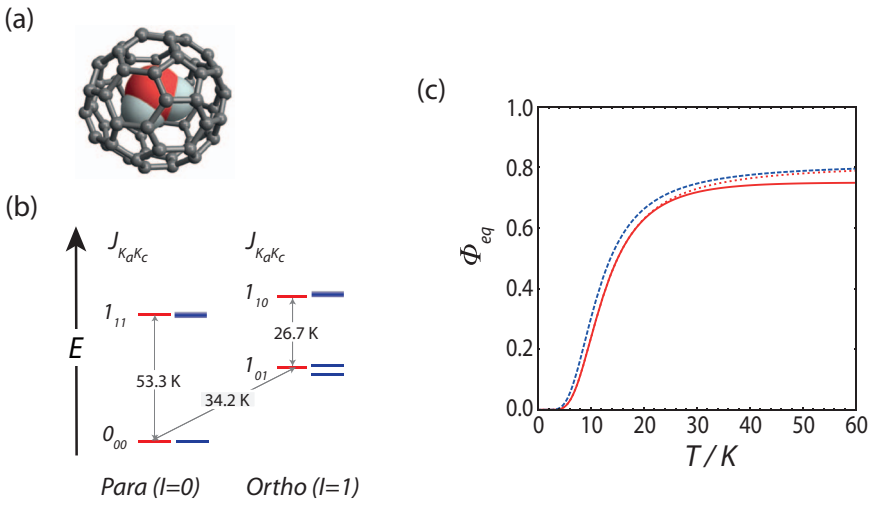

FIG. 1. (a) Molecular structure of the water-endofullerene $H_2O@C_{60}$ and (b) the lowest rotational levels of the water molecule. The *para* and *ortho* energy levels are shown for H_2O in the gas phase (red)[13] and in the solid endofullerene (blue).[42] The shading indicates unresolved fine structure. Energies are given in temperature units. (c) The temperature dependence of the equilibrium fractional population Φ_{eq} of *ortho*-H_2O, calculated from the energy levels of H_2O in the gas phase[13] is shown by the red solid curve. The dashed lines show the fractional *ortho*-populations calculated by considering only the four lowest energy levels of free water (dotted, red) and endohedral water[42] (dashed, blue). For these two curves the incomplete convergence to the high temperature value of 3/4 is related to the unaccounted higher energy levels in Eq. (1).

supramolecular compound $H_2O@C_{60}$ (see Figure 1(a)). This material has been synthesized in macroscopic quantities by a multistep chemical procedure.[40,41] It is a black solid which is stable under a wide range of physical conditions and is very convenient to handle. The C_{60} cage provides a robust and uniform environment which allows free rotation of the endohedral water molecules under a very wide range of conditions.

The behaviour of the endohedral water molecules in $H_2O@C_{60}$ has been studied by a variety of spectroscopic methods, including NMR, inelastic neutron scattering, and infrared spectroscopy.[42] The rotational energy levels of the endohedral H_2O are very similar to those in the gas phase, indicating free rotation of the water, even at cryogenic temperatures.[42] Spin-isomer conversion was followed by equilibrating the sample at high temperature, cooling to low temperature, and following the spin isomer conversion by infrared spectroscopy and inelastic neutron scattering.[42] The spin conversion process takes several hours at temperatures below ~10 K. However, although neutron scattering and infrared spectroscopy provide a clear signature of spin isomer conversion, it is difficult to obtain detailed kinetic information. Neutron scattering suffers from poor time resolution, while the quality of the infrared data is compromised by the overlapping absorption bands from several different transitions.

This paper concerns nuclear magnetic resonance (NMR) observations of spin isomer conversion in $H_2O@C_{60}$. A strength of NMR is that the interpretation of the data is relatively unambiguous, since the NMR signals of the endohedral *ortho*-H_2O can be easily distinguished from other signals deriving from residual impurities or from the background of the apparatus. In addition, the good time resolution and high signal-to-noise ratio of the NMR measurements, especially when compared to neutron scattering, allows an accurate representation of the kinetics of spin isomer conversion. A disadvantage of NMR with respect to infrared spectroscopy and neutron scattering is that the *para* spin isomer has nuclear spin $I = 0$ and cannot be observed. The spin conversion process must be followed by a change in intensity of the *ortho*-H_2O NMR signal.

As shown below, the kinetic evidence from NMR indicates that the *ortho* to *para* conversion of $H_2O@C_{60}$ is a bimolecular process, involving the interaction between pairs of neighbouring *ortho* spin isomers.

NMR is able to probe the environment of the water molecules through double-resonance experiments. This allows evaluation of the role of nearby magnetic nuclei in spin-isomer conversion, as has been postulated in related systems.[43,44] In the current case, cross-polarization experiments indicate that the interactions between the H_2O protons and the ^{13}C nuclei in the enclosing fullerene cage play a negligible role in the *ortho-para* conversion of water in $H_2O@C_{60}$. Some observations on the possible spin-isomer conversion mechanism in $H_2O@C_{60}$ are given at the end of this paper.

II. ^{1}H NMR AND *ORTHO-PARA* CONVERSION

A. Energy levels and spin isomers

The energy levels of $H_2O@C_{60}$ have been studied by inelastic neutron scattering, IR and NMR.[42] The water molecules enjoy full rotational freedom even at cryogenic temperatures. The four lowest H_2O rotational energy levels in $H_2O@C_{60}$ are compared to the gas phase levels in Figure 1(b). The main effect of the fullerene encapsulation, is a ~0.6 meV splitting of the three-fold degenerate ground-state *ortho* level 1_{01}, observed directly by inelastic neutron scattering.[42] The lifting of degeneracy implies a breaking of local inversion symmetry, which is consistent with observations of an intramolecular dipole-dipole interaction between the water protons, as revealed by solid-state NMR.[42] The origin of the lifted degeneracy is currently unknown but may be due to a

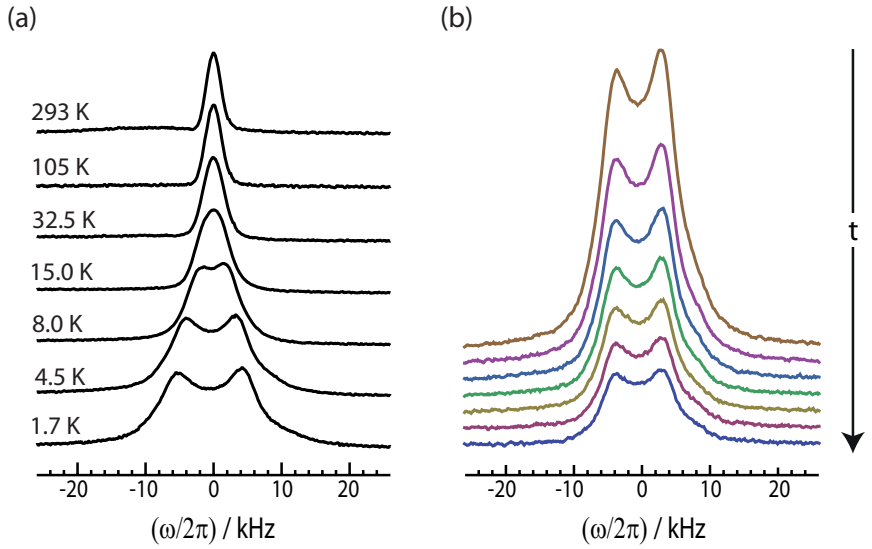

FIG. 2. ^{1}H spectra of $H_2O@C_{60}$. (a) ^{1}H spectra from room temperature down to 1.7 K. (b) ^{1}H spectra recorded at a set temperature of 5 K, taken at intervals of 2.25 h after cooling from 60 K. During all the experiments the temperature was stabilized to 5 K within 0.1 K. The first spectrum (top) was taken after waiting 30 min, in order to allow thermal equilibration of the equipment.

spontaneous symmetry-breaking in the $H_2O@C_{60}$ system, associated with a coupling between the H_2O electric dipole moment and the electric charge distribution in the fullerene cage, analogous to the Jahn-Teller effect.[42]

Denote the fractional population of *ortho*-H_2O by Φ, so that the fractional population of *para*-H_2O is $1 - \Phi$. In thermal equilibrium at temperature T, the spin-isomer populations are governed by the Boltzmann distribution:

$$\Phi_{eq}(T) = Z(T)^{-1} \sum_o g_o \exp(-E_o/k_B T), \qquad (1)$$

where the partition function is

$$Z(T) = \sum_o g_o \exp(-E_o/k_B T) + \sum_p g_p \exp(-E_p/k_B T) \qquad (2)$$

and the spin degeneracies are $g_o = 3$ and $g_p = 1$. The sums are taken over the *ortho* energy levels (subscript o) and *para* energy levels (subscript p). The temperature dependence of $\Phi_{eq}(T)$ follows a sigmoidal curve increasing rapidly from 0 at low temperature to $\Phi_{eq} \simeq 3/4$ above 50 K. The steepest gradient of Φ_{eq} with respect to temperature is around 15 K (see Figure 1(c)). Spin-isomer conversion may therefore be induced by changing the sample temperature between values on either side of ∼15 K.

B. ^{1}H NMR

Since *ortho*-H_2O has total nuclear spin $I = 1$, while *para*-H_2O has total nuclear spin $I = 0$, only the *ortho*-H_2O species generate a ^{1}H NMR signal.

Figure 2(a) shows the proton line shape of $H_2O@C_{60}$ as a function of temperature, on samples in full thermal equilibrium. At high temperature, the proton spectrum resembles a single Gaussian peak with width at half height of about 2 kHz. The peak broadens when the temperature is reduced. Below ∼15 K, the peak splits into a slightly asymmetric doublet. The splitting is due to dipolar interactions between the water protons in *ortho*-H_2O, associated with the lifted degeneracy of the ground rotational state 1_{01}, as shown in Figure 1(b). There is also a minor chemical shift anisotropy effect, possibly caused by an asymmetric perturbation of the electron density in the cage.[45] The low-temperature dipole-dipole coupling in $H_2O@C_{60}$ has also been observed by cryogenic magic angle spinning NMR.[42] The dipolar splitting is not relevant to the spin conversion, and will not be discussed further.

Figure 3 shows the ^{1}H spin-lattice relaxation time constant T_1 for $H_2O@C_{60}$, as a function of inverse temperature, measured by a standard saturation-recovery procedure. The ^{1}H T_1 values are less than 5 s over the full temperature range, reflecting the high mobility of the endohedral H_2O molecules. The T_1 minimum at ∼8 K is probably associated with the ∼0.6 meV splitting of the *ortho*-$H_2O@C_{60}$ ground rotational state (see Figure 1(b)).

C. Spin isomer conversion

At constant temperature, the amplitude of the NMR signal is proportional to the concentration of *ortho*-water in the

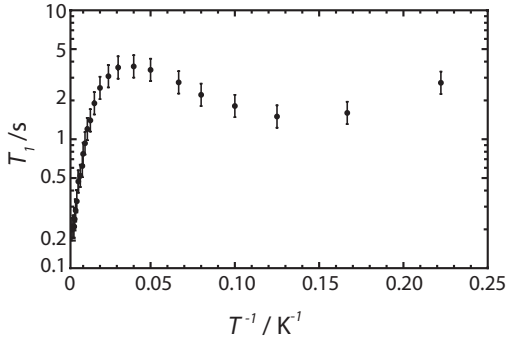

FIG. 3. ^{1}H spin-lattice relaxation times T_1 as a function of inverse temperature for $H_2O@C_{60}$, in a magnetic field of 14.1 T. The vertical axis uses a logarithmic scale.

sample. A slow change in the ^{1}H NMR signal amplitude with time, at constant temperature, is indicative of *ortho-para* conversion.

The spectra in Figure 2(b) were obtained as follows: First, the sample was equilibrated for many hours at a temperature of 60 K. At this temperature the equilibrium ratio of *ortho* to *para*-water is approximately 3 to 1 (see Figure 1(c)). The sample temperature was reduced to 5 K and the apparatus was left to equilibrate for 30 min. The first ^{1}H spectrum was taken by applying a single radio frequency pulse and taking the Fourier transform of the response (top spectrum in Figure 2(b)). Since the equilibrium fraction of *ortho*-water is extremely small at this temperature, the NMR signal is due to metastable *ortho*-water molecules which have not yet converted to the NMR-silent *para* state. Subsequent spectra were recorded using a single ^{1}H pulse, every 2.25 h. Since T_1 is only a few seconds (see Figure 3), the slow decay in intensity cannot be associated with saturation of the nuclear magnetization by the infrequent radiofrequency pulses. The gradual reduction in the signal intensity with time indicates slow spin conversion from *ortho*-H_2O to *para*-H_2O, over a timescale of hours.

At a given sample temperature T, the NMR signal is proportional to the instantaneous *ortho* fraction Φ, and also the inverse temperature T^{-1}, through the Curie law for the nuclear magnetization. The ^{1}H NMR signal intensity from $H_2O@C_{60}$, at an arbitrary time t and sample temperature T, may be written:

$$I_{\mathrm{NMR}}(T,t) \propto C(T)T^{-1}\Phi(t), \tag{3}$$

where $\Phi(t)$ may differ from $\Phi_{eq}(T)$ in the case that spin-isomer conversion is not complete. The instrumental factor $C(T)$ takes into account the temperature-dependent performance of the tuned detection circuit. Equation (3) assumes that the nuclear spin system comes to internal equilibrium much faster than the spin-isomer conversion process. Since the proton T_1 is only a few seconds (see Figure 3), while spin-isomer conversion takes tens of minutes or longer, this is a good approximation for the experiments described here.

Figure 4 shows the variation of the NMR signal intensity when the sample temperature was equilibrated at 50 K, changed from 50 K to 5 K over about 30 min, maintained at 5 K for several hours, and then raised to 32.5 K. Before the start of the experiment ($t = 0$), the sample was equilibrated for many hours at 50 K. The NMR signal intensity was constant until the temperature was reduced to 5 K. The cooling and stabilization of the probe required about 30 min. The strong increase in the NMR signal intensity upon cooling is due to the Curie term T^{-1} in Eq. (3), corresponding to the increased polarization of the nuclear spins at low temperature, and is unrelated to *ortho-para* conversion. The subsequent slow decay of the NMR signal intensity at the constant temperature of 5 K, over a duration of many hours, reflects the conversion of *ortho*-water into *para*-water. After monitoring the signal for about 10 h at 5 K, the temperature was rapidly increased to 32.5 K. The sudden reduction of the signal intensity is again due to the Curie factor T^{-1} and is unrelated to spin-isomer conversion. The subsequent recovery of the NMR signal is due to back-conversion of *para*-H_2O to *ortho*-H_2O, as a new

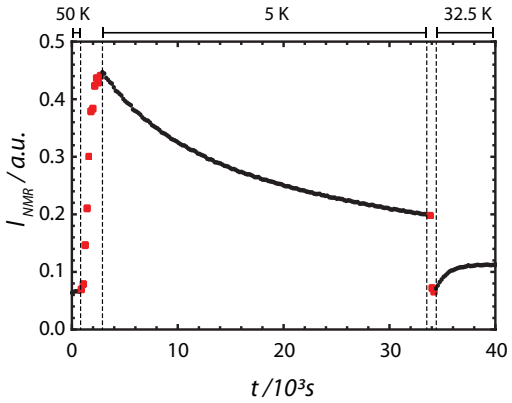

FIG. 4. Integrated ^{1}H NMR signal intensity I_{NMR} as function of time during an experiment involving two temperature jumps, on a sample of $H_2O@C_{60}$. ^{1}H NMR spectra were recorded at time intervals of 180 s, using a saturation-recovery procedure to ensure a well-controlled nuclear magnetization (see Sec. IV). The sample temperature is reported at the top of the graph. Integrated NMR signals recorded at a constant temperature are shown as black dots, while those recorded during a temperature change are reported as red squares.

thermal equilibrium is reached at the relatively high sample temperature of 32.5 K.

These results demonstrate that H_2O nuclear spin conversion in $H_2O@C_{60}$ may be observed with excellent signal-to-noise ratio and time resolution by monitoring the ^{1}H NMR signal after a temperature jump.

D. Spin-isomer conversion kinetics

Figures 5(a) and 5(b) show the experimental decays in the ^{1}H NMR signal amplitude of $H_2O@C_{60}$ after full thermal

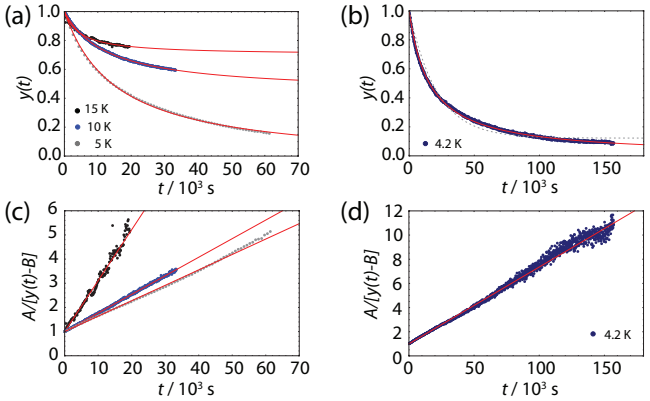

FIG. 5. Integrated ^{1}H NMR signals of $H_2O@C_{60}$, as a function of time, after equilibration at a temperature of 60 K and (a) cooling to 15 K (black dots), 10 K (blue dots), 5 K (gray dots) at a field of 14.1 T and (b) cooling to 4.2 K at a field of 0.86 T. The vertical scale is the integrated NMR signal amplitude normalised to its initial value, $y(t) = I_{\mathrm{NMR}}(t)/I_{\mathrm{NMR}}(0)$. The NMR data are shown by dots with the best fit to Eq. (6) shown by solid lines, where A and κ are fit parameters given in Table I and $B = 1 - A$. In panel (b), the gray dashed line is the best fit of the experimental points to an exponential decay. Panels (c) and (d) show the data transformed so as to provide straight-line plots for second-order kinetics. The signal was monitored via direct acquisition of the proton signal using the sequence in Figure 8(a) with a recycle delay between transients of 60 s for the experiments in panel (a) and 120 s for the experiment in panel (b).

equilibration at a temperature of 60 K and cooling to temperatures in the range 4 K to 15 K, in two different magnetic fields.

Previous studies of spin isomer conversion for H_2O in inert gas matrices have observed exponential decays characteristic of a first-order process.[43] However the data in Figure 5 do not match an exponential form. This is readily seen in Figure 5(b) where the decay is too steep at the beginning and too slow at the end to be described by a single exponential.

Second-order kinetic behaviour has been observed for the *ortho-para* conversion of H_2 in the solid state.[1,46–49] We therefore explored the fitting of the NMR data to a second-order spin-conversion process, according to the rate equation:

$$\frac{\mathrm{d}\,\Delta\Phi}{\mathrm{d}\,t} = -k_2\Delta\Phi^2, \tag{4}$$

where k_2 is the second-order rate constant, and $\Delta\Phi = \Phi - \Phi_{eq}$ is the deviation of the *ortho* fraction from equilibrium at the sample temperature. The solution of Eq. (4) is

$$\Delta\Phi(t)^{-1} = \Delta\Phi(0)^{-1} + k_2 t, \tag{5}$$

where $\Delta\Phi(0) = \Phi(0) - \Phi_{eq}$ is the initial deviation of the *ortho* fraction from equilibrium. At constant temperature the NMR signal $I_{\mathrm{NMR}}(t)$ is proportional to the *ortho* fraction Φ. This leads to the following relationship for the normalised NMR signal intensity, defined as $y(t) = I_{\mathrm{NMR}}(t)/I_{\mathrm{NMR}}(0)$:

$$y(t) = A(1 + \kappa t)^{-1} + B, \tag{6}$$

where $A + B = 1$, $A = \Delta\Phi(0)/\Phi(0)$, $B = \Phi_{eq}/\Phi(0)$ and $\kappa = \Delta\Phi(0)k_2$.

According to Eq. (6), a plot of $A/(y(t) - B)$ against t should be a straight line with slope κ. The corresponding transformations of the NMR data are shown in Figures 5(c) and 5(d). In each case, the independent parameters A and κ were adjusted to obtain the best straight-line fit using the constrain $B = 1 - A$. A good fit to the second-order kinetic law is found in all cases. The fit parameters and their confidence limits are shown in Table I.

The second-order rate constant may be estimated from the slope κ of the straight-line plot through the relationship $k_2 = \kappa/\Delta\Phi(0) = \kappa/[A\Phi(0)]$ where $\Delta\Phi(0)$ is the deviation of *ortho* fraction from equilibrium at time point $t = 0$. Unfortunately this initial deviation is hard to estimate accurately with the current apparatus, since it takes several tens of minutes for the sample to cool and the temperature to stabilise, with *ortho-para* conversion proceeding at an unknown rate during the cooling interval. To obtain rough estimates of the second-order rate constant k_2 (last column in Table I), we assumed that $\Phi(0)$ is between 0.50 and 0.75, with the upper value corresponding to thermal equilibrium at the higher temperature before cooling has taken place.

The estimated values in the last column of Table I indicate a temperature-dependent second-order process at low temperature, with a rapid increase in k_2 when the temperature is raised above 10 K. There is no evidence of a dependence on the static magnetic field strength.

TABLE I. Best-fit second-order rate parameters for *ortho-para* conversion in $H_2O@C_{60}$ at four different temperatures and at two magnetic fields. The kinetic parameters refer to Eq. (6). The values of k_2 were estimated from the relation $k_2 = \kappa/[A\Phi(0)]$ using the assumption $0.5 \le \Phi(0) \le 0.75$ for the initial value of the *ortho* fraction from equilibrium.

T/K	B/T	$\kappa/(10^{-6}\ \mathrm{s}^{-1})$	A	$k_2/(10^{-6}\ \mathrm{s}^{-1})$
15	14.1	210 ± 10	0.30 ± 0.02	1200 ± 250
10	14.1	77 ± 3	0.56 ± 0.01	230 ± 50
5	14.1	64 ± 2	1.04 ± 0.03	100 ± 20
4.2	0.86	63 ± 2	1.00 ± 0.01	105 ± 20

III. ^{13}C NMR

It has been postulated that spin-isomer conversion may be catalyzed by neighbouring magnetic nuclei.[43,44] In the current case of $H_2O@C_{60}$, this seems unlikely, since the kinetic evidence presented above indicates a dominant second-order process, which appears to be inconsistent with catalysis by extraneous nuclei. Nevertheless, it is of interest to explore whether natural abundance ^{13}C nuclei in the C_{60} cages do influence the water spin conversion.

Since the natural abundance of ^{13}C is 1.07%, 48% of the C_{60} cages contain at least one ^{13}C nucleus. In principle, the role of ^{13}C could be studied by preparing $H_2O@C_{60}$ samples which are either enriched or depleted in ^{13}C, and comparing the nuclear spin conversion kinetics with the non-enriched material. That would be an expensive and laborious process. Fortunately, the involvement of ^{13}C may also be explored without preparation of labelled or depleted material, by using Hartmann-Hahn cross-polarization (CP)[50,51] to transfer magnetization from the endohedral *ortho*-H_2O protons to nearby ^{13}C nuclei.

When the ^{1}H NMR signals are observed directly, almost equal contributions are made by H_2O molecules in C_{60} cages containing no ^{13}C nuclei, and those containing at least one ^{13}C. In contrast, when cross-polarization from ^{1}H to ^{13}C is conducted under conditions that only allow short-range magnetization transfer, the resulting ^{13}C signals are derived exclusively from C_{60} cages that contain at least one ^{13}C nucleus, and which also encapsulate an *ortho*-H_2O molecule. Any catalysis of spin conversion by ^{13}C would show up as a difference in the spin-isomer conversion trajectories, as measured by ^{1}H NMR and by cross-polarized ^{13}C NMR.

Figure 6(a) shows a set of cross-polarized (CP) ^{13}C spectra, acquired at a temperature of 5 K using Hartmann-Hahn contact times τ_{CP} equal to 1 ms, 5 ms, and 10 ms. For the longer contact times, the ^{13}C spectrum is roughly consistent with the theoretical line shape for randomly-oriented static chemical shift anisotropy (CSA) tensors, with principal values as reported in the literature,[52,53] and shown in Figure 6(b). These spectra show that the rotational motion of the $H_2O@C_{60}$ cages is suppressed at cryogenic temperatures, as is well-known for C_{60} itself.[52]

The CP spectrum with short contact time $\tau_{CP} = 1$ ms displays a strong loss of signal intensity in the region around the isotropic chemical shift value of 143 ppm (Figure 6(a), lower spectrum). This selective loss of intensity at short τ_{CP} can be understood from the following observations. (1) For small values of τ_{CP}, the transfer of polarization is short-range. To

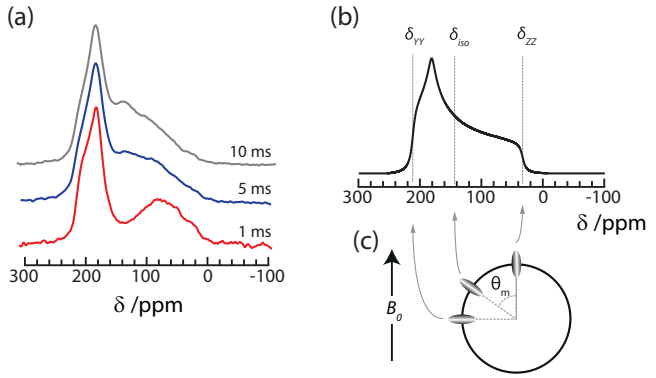

FIG. 6. (a) ^{13}C CP spectra acquired with contact times $\tau_{CP} = 10$ ms (top, gray), 5 ms (middle, blue), and 1 ms (bottom, red), without proton decoupling during signal acquisition, at a magnetic field of 14.1 T. (b) Simulated static CSA pattern of C_{60} using the principal values reported in the literature ($\delta_{XX} = 182$ ppm, $\delta_{YY} = 213$ ppm, $\delta_{ZZ} = 33$ ppm).[52] (c) Schematic representations of the ^{13}C CSA tensors at three different positions in the fullerene cage. The three ^{13}C sites give rise to peaks at the indicated spectral frequencies, assuming a magnetic field in the vertical direction, the most shielded principal axis Z oriented along the cage radius and the less shielded axis Y oriented perpendicular to the plane of the figure, respectively. The ^{13}C nuclei at the "magic angle" $\theta_m = \arctan\sqrt{2}$ resonate at the isotropic chemical shift δ_{iso}.

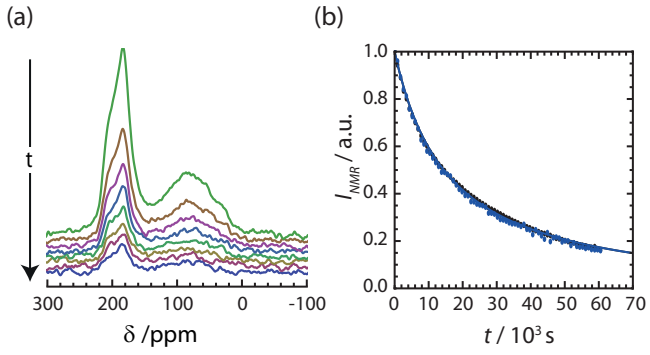

FIG. 7. (a) ^{13}C spectra of $H_2O@C_{60}$ (with $f = 0.9$) at a temperature of 5 K and a magnetic field of 14.1 T, recorded at time intervals of 2.25 h, after fast cooling from 60 K, and waiting 30 min for thermal equilibration of the apparatus. The ^{13}C signals were obtained by CP from ^{1}H nuclei using a contact time $\tau_{CP} = 1$ ms. (b) Decay as function of time for two sets of integrated NMR signals: directly observed ^{1}H NMR signals (black squares), and ^{13}C CP signals obtained with $\tau_{CP} = 1$ ms (blue dots). The solid line indicates the fit of the proton data to Eq. (6).

a good approximation, the ^{1}H magnetisation of *ortho*-H_2O is exclusively transferred to ^{13}C nuclei located in the same fullerene cage. (2) The rate of polarization transfer depends on the secular component of the heteronuclear dipole-dipole interaction, which depends on the angle θ_{CH} between the ^{1}H-^{13}C internuclear vector and the magnetic field, according to the angular factor $P_2(\cos\theta_{CH}) = (3\cos^2\theta_{CH} - 1)/2$.[54] Since the quantum wavefunction of the endohedral H_2O is localized near the center of the cage, the angle θ_{CH} is close to the angle subtended by the radial vector from the cage centre to the carbon position, and the applied magnetic field. The cross-polarization from *ortho*-H_2O to ^{13}C is inefficient for ^{13}C sites located such that the radial vector θ_{CH} is close to the magic angle $\theta_m = \arctan\sqrt{2}$. (3) The ^{13}C CSA tensor in C_{60} has a small biaxiality ($\eta = 0.28$).[52] (4) *Ab initio* calculations predict that the unique principal axis corresponding to the most shielded value subtends the small angle of 11.8° with the radial vector.[55] To a good approximation, the ^{13}C CSA tensors in C_{60} may therefore be visualised as ellipsoids with their long axes parallel to the cage radii (Figure 6(b)). (5) It follows that in $H_2O@C_{60}$ the rate of ^{1}H-^{13}C polarization transfer and the ^{13}C chemical shift are highly correlated. ^{13}C sites which resonate close to the isotropic chemical shift also have an angle θ_{CH} close to the magic angle, and therefore suffer from weak polarization transfer. This gives rise to a strong loss of spectral intensity around the isotropic ^{13}C chemical shift.

The observed "magic-angle hole" in the short-τ_{CP} ^{13}C spectra therefore provides strong confirmation that the cross-polarization is local to each $H_2O@C_{60}$ molecule. These are exactly the conditions required to examine the influence of ^{13}C on *ortho-para* conversion.

Figure 7(a) shows the decay in the ^{13}C CP signals due to *ortho-para* conversion of the endohedral H_2O, after a change in sample temperature from 60 K to 5 K, using a short contact interval $\tau_{CP} = 1$ ms. The decay in the cross-polarized ^{13}C spectral amplitude is indistinguishable from that of the directly observed ^{1}H signal, as shown by the superimposed curves in Figure 7(b). We conclude that the ^{13}C nuclei have no significant influence on the spin-isomer conversion of H_2O in the case of $H_2O@C_{60}$.

IV. MATERIALS AND METHODS

A. Sample preparation

$H_2O@C_{60}$ was prepared by the "molecular surgery" synthetic method.[40,56] A set of chemical reactions is used to open an orifice in each fullerene cage, by adding exohedral groups to the cage. Water molecules are inserted into the open-cage fullerene molecules and the external shell reconstituted.

Preparations of $H_2O@C_{60}$ are typically solid solutions containing $H_2O@C_{60}$ as well as empty C_{60} cages. The "filling factor" f specifies the fraction of cages that are filled with water. The synthetic procedure described above led to a sample of $H_2O@C_{60}$ with $f \simeq 0.7$. This sample was enriched further by several cycles of high-performance liquid chromatography (HPLC). All experiments reported in this paper used a sample with a filling factor $f = 0.9$, as estimated by integrating the HPLC peaks corresponding to the empty and water-filled fullerenes.

The sample was purified by sublimation to remove occluded impurities and solvents. The description of the sublimation apparatus and procedure will be reported elsewhere.[41] Finally the sample was placed in Pyrex tubes, evacuated for several hours and sealed under vacuum. In all the cases, the fullerenes contained ^{13}C nuclei in natural abundance.

About 7 mg of material were used for the experiments at 14.1 T. For the low field experiments (0.86 T) about 60 mg were used.

B. NMR equipment

The 14.1 T NMR spectra were obtained using a Bruker AVANCE-II+ spectrometer and a home-built NMR probe

with a 2 mm diameter solenoid. The NMR probe was mounted in an Oxford Instruments continuous-flow cryostat (spectrostatNMR) using helium coolant. An insulated transfer line was used to drive the cold He gas from a 60 L Dewar into the cryostat. The He flow rate could be adjusted up to a value of 2.5 litres per hour and its temperature was regulated by a thermo-resistance heater placed close to the sample. No sample rotation was used.

A calibrated Cernox sensor (accuracy of ±0.15 K), in good thermal contact with the sample container (2 mm Pyrex tube) and isolated from the cold helium gas stream, was used as an indicator of the sample temperature. The temperature calibration procedure is described elsewhere.[57]

The sample temperature was left to stabilize at 50 K for about one hour before inducing spin-isomer conversion by changing the temperature. In the 14.1 T apparatus, the cooling from 50 K to any temperature below 20 K took between 30 and 60 min while warming and stabilization from 5 K to any temperature up to 60 K took between 5 and 10 min.

The NMR data recorded at 0.86 T were obtained using a TecMag Apollo spectrometer and a superconducting magnet system supplied by Cryogenic Ltd. The latter incorporated a helium cryostat with the sample accommodated inside a home-built cryogenic NMR probe. The 90° pulse length was 2 μs and the ring-down time was 7 μs. For the duration of the experiment, extending to two days, the magnet was permanently energised at constant current by a stabilised power supply. For the magnetisation vs. time experiments, the final stage of the sample cooling process between 30 K and 4.2 K took approximately 6 min. The time between measurements of magnetisation was long compared with T_1.

C. NMR experiments

^{1}H spectra were acquired using a pulse sequence composed by a saturation comb of 200 90° pulses separated by 100 μs on the proton channel, followed by a recovery delay τ, followed by a single 90° pulse, a ring-down delay of 5 μs, and signal detection (see Figure 8(a)). The durations of the 90° pulses were adjusted at each temperature, varying from 7 μs at room temperature to 3.6 μs for all the spectra below 50 K. The ^{1}H chemical shift scale was calibrated by setting the narrow room-temperature ^{1}H resonance of $H_2O@C_{60}$ to −4.8 ppm.

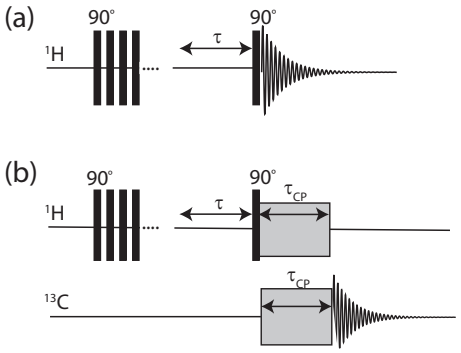

FIG. 8. Pulse sequences used for the NMR experiments: (a) Pulse sequence for direct observation of ^{1}H spectra. (b) Pulse sequence used for observation of ^{13}C spectra. The saturation combs typically employed 200 90° pulses separated by 100 μs on the ^{1}H channel.

The sequence of Figure 8(a) was used to measure ^{1}H spin-lattice relaxation times by monitoring the integrated NMR signal as function of the delay τ. For each temperature T, the spin-lattice relaxation time T_1 was obtained by fitting the experimental recovery curve to the exponential saturation-recovery law $I_{NMR}(\tau) = a + b[1 - \exp(-\tau/T_1)]$.

A recovery delay of $\tau = 60$ s was used between transients when monitoring spin conversion at 15, 10, and 5 K. A recovery delay of $\tau = 120$ s was used in the experiment at 4.2 K. These recovery delays are much longer than the measured proton spin-lattice relaxation time T_1 at all temperatures, see Figure 3.

^{13}C spectra were acquired using cross-polarization from ^{1}H with no decoupling during acquisition, preceded by saturation pulses on the proton channel followed by a recovery delay τ (see Figure 8(b)). Three sets of measurements were performed with contact intervals τ_{CP} of 1, 5, and 10 ms. The ^{13}C chemical shift scale was calibrated by setting the narrow room-temperature ^{13}C resonance of $H_2O@C_{60}$ to 144 ppm.

D. Simulations

The numerical simulations shown in Figure 10 were obtained by a similar method to the studies of percolation networks.[58] The network is represented by an object in Python which consists of a list of nodes represented by indices (i, j, k), each index ranging from 0 to 19. Each node corresponds to a C_{60} cage. When the network is initialized, each node is filled with a water molecule with probability $f = 0.9$, corresponding to the substance used in the experiments. Initially, each filled node is added to the lists of *ortho* and *para* molecules with probabilities of 75% and 25%, respectively, corresponding to the room temperature equilibrium ratio.

The neighbours of each node are obtained by changing two of the node's indices by ±1, so that each node has 12 neighbours, corresponding to the FCC lattice. Periodic boundary conditions are used.

To study the conversion of *ortho* to *para* molecules, the network is propagated in time as follows: (1) at each step, iterate over all the *ortho* molecules; (2) for each *ortho* molecule, find all neighbouring cages that also contain an *ortho* molecule; (3) with probability $p = 1\%$ change the molecule and its neighbour to *para*; and (4) if the change took place, go to the next molecule in the list of *ortho* molecules. One *ortho* molecule may be part of multiple pairs and, if no flip occurs, the algorithm will also revisit those *ortho* molecules which have already been tested against their neighbours. In Figure 10(b), the exchange of neighbouring *ortho-para* molecules with probability 1% is also implemented.

No back-conversion from *para* to *ortho* is included in the simulations shown in Figure 10. We have also implemented simulations which include this process, which is significant at higher temperatures. No unusual effects were observed.

V. DISCUSSION

The NMR evidence described above indicates that: (1) the *ortho-para* conversion process in $H_2O@C_{60}$ follows

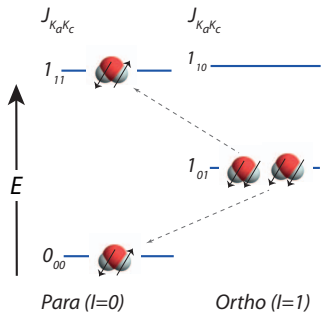

FIG. 9. Schematic representation of the spin conversion process in $H_2O@C_{60}$ in which two molecules of *ortho*-H_2O convert into two *para*-H_2O molecules. The process shown is the most energetically favorable among the bimolecular processes since the *ortho* state 1_{01} is half-way in energy at 2.3 meV between the two para states 0_{00} and 1_{11} separated by 4.6 meV.[42]

a second-order rate law; (2) at temperatures below ∼10 K, the conversion kinetics are temperature-independent; and (3) the ^{13}C nuclei in the cage do not play a significant role in the spin-isomer conversion of H_2O.

The second-order kinetic rate law suggests a bimolecular process in which neighbouring *ortho*-H_2O pairs interact at close range. We propose a bimolecular mechanism of the form

$$o + o \rightarrow p + p^*, \tag{7}$$

where the left-hand side indicates a pair of neighbouring $H_2O@C_{60}$ molecules, each containing *ortho*-H_2O. Equation (7) suggests that the neighbouring *ortho*-$H_2O@C_{60}$ molecules may interact to generate a pair of *para*-$H_2O@C_{60}$ molecules. The asterisk indicates the generation of a *para*-H_2O in a rotationally excited state. This is required for energetic reasons (see Figure 9). After conversion the excess energy of the p^* molecule is rapidly dissipated to the lattice.

It is well-known that bimolecular processes give rise to second-order kinetics in the case of solution-state chemical reactions, where reagents freely diffuse in space. It is less obvious whether this also applies to a three-dimensional solid, where the molecules are fixed in space.

To investigate this issue we performed numerical simulations using a simple lattice automaton, based on a model in which each H_2 molecule interacts only with the nearest neighbours in the crystalline phase of C_{60},[59,60] with 90% of lattice sites occupied by a C_{60} molecule containing an endohedral water, as in the experimental situation. At the start of the simulation, 75% of the available $H_2O@C_{60}$ sites are assigned as *ortho*, with the remaining 25% set as *para*. This corresponds to the high-temperature *ortho-para* ratio. On each simulation step, neighbouring *ortho* pairs have a 1% chance of converting to a pair of *para* molecules.

Figure 10(a) shows the conversion kinetics generated by this process. The linearised representation of the second-order kinetics, shown in Figure 10(a), shows that the process initially follows a second-order rate law to a good approximation, but that strong deviations are observed at long times, when the fraction of remaining *ortho* molecules becomes low. The conversion becomes "stuck" since a significant fraction of *ortho* molecules are left without a nearby *ortho* partner, and cannot convert.

The long-term persistence of "stuck" *ortho*-H_2O molecules is not observed for $H_2O@C_{60}$. There are several

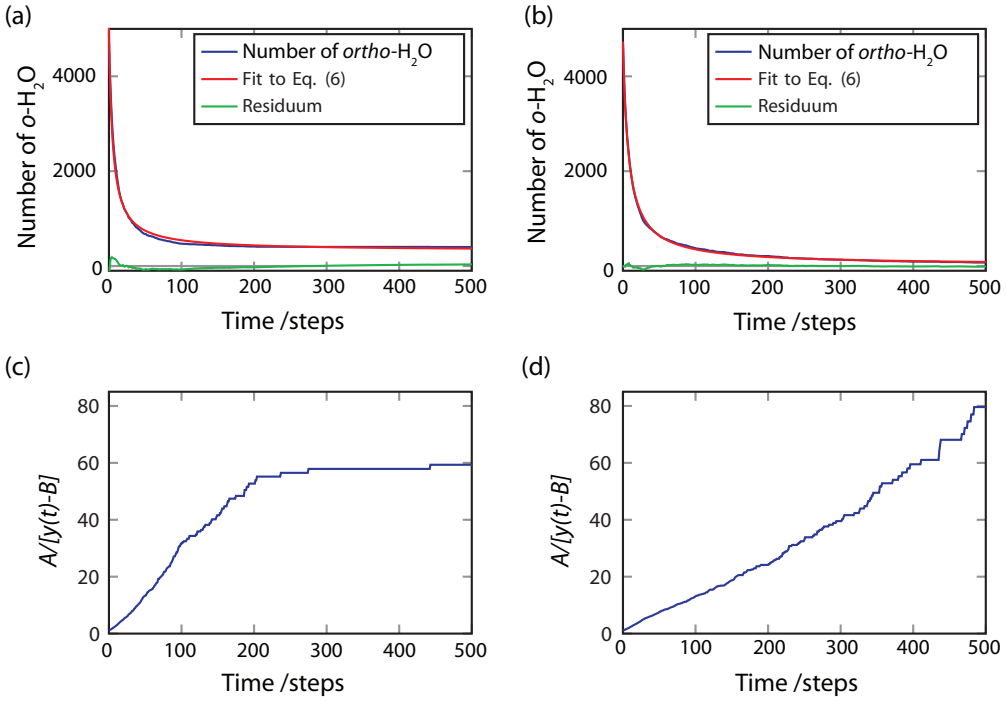

FIG. 10. Numerical simulation of the conversion process. In (a), the network is propagated by converting pairs of neighbouring *ortho* molecules into *para* molecules with a probability of 1% at each time step as discussed in Sec. IV D. In (b), in addition neighbouring *ortho* and *para* molecules may exchange state so that isolated *ortho* molecules can diffuse through the network until they can pair with another *ortho* molecule and relax into *para* H_2O, leading to complete conversion of the sample. (c) and (d) show the linearisation of the simulated data as in Figure 5: the parameters *A* and *B* were obtained from the best fit of the simulated dataset with Eq. (6).

possible explanations for this: (1) the $o + o \rightarrow p + p^*$ conversion process may take place at distances much larger than a nearest-neighbour approach; and (2) a second process occurs which allows *ortho* molecules to "diffuse" through the lattice, and "find" an *ortho* partner, allowing recombination. Indeed, in the case of H_2, such diffusion processes are known to occur.[47,48,61,62]

There can be no *physical* diffusion of *ortho*-$H_2O@C_{60}$ through the low-temperature lattice. However, it is plausible that neighbouring *ortho* and *para* molecules have a finite probability of exchanging identity, i.e.,

$$o + p \rightarrow p + o. \tag{8}$$

This process generates a form of *spin diffusion*, analogous to the diffusion of tunnelling energy in solids containing unhindered methyl rotors.[63] Figure 10(b) shows the result of a lattice automaton simulation in which the processes in Eqs. (7) and (8) occur with equal probability. As expected, the *ortho-para* exchange process in Eq. (8) allows diffusion of isolated *ortho* molecules through a *para*-rich lattice, allowing them to find a *ortho* partner and accomplish spin conversion. When this process is included, second-order kinetics is followed fairly accurately out to long times.

The experimental observation of second-order kinetics for the spin conversion in $H_2O@C_{60}$ is therefore consistent with a bimolecular spin conversion mechanism for neighbouring endohedral *ortho*-H_2O molecules, combined with a spin-diffusion-like process allowing exchange of *ortho* and *para* identities between neighbouring molecules. However we cannot exclude alternatives to spin diffusion, such as the presence of a longer range $o + o \rightarrow p + p^*$ process.

The processes in Eqs. (7) and (8) provide a plausible explanation for the second-order kinetics of spin isomer conversion in $H_2O@C_{60}$. But what is the microscopic mechanism for these processes?

In the case of H_2, spin isomer conversion is induced by magnetic fields that are inhomogeneous on a molecular scale.[46,64] Since *ortho*-H_2O possesses a nuclear magnetic moment, while *para*-H_2O does not, it is plausible that magnetic dipole-dipole interactions between the ^{1}H nuclei of H_2O molecules in neighbouring cages provide a mechanism for the bimolecular conversion process in Eq. (7). However, such interactions are exceedingly small due to the relatively large size of the cages. Furthermore, the experiments described above indicate that ^{13}C nuclei on the same cage as the endohedral H_2O do not cause significant *ortho-para* conversion. Although ^{13}C is less magnetic than ^{1}H, a ^{13}C nucleus in the same cage is much closer to an endohedral proton than an endohedral neighbour. The magnetic dipole coupling between protons in neighbouring cages is $(\mu_0/8\pi^2)\hbar\gamma_H^2 r_{HH}^{-3} \approx -120$ Hz where r_{HH} is the proton-proton distance (estimated to be $r_{HH} \approx 10$ Å) and γ_H is the proton magnetogyric ratio. The coupling between a proton at the center of a cage and a ^{13}C nucleus inside the same cage is $(\mu_0/8\pi^2)\hbar\gamma_H\gamma_C r_{CH}^{-3} \approx 700$ Hz, where γ_C is the magnetogyric ratio for ^{13}C. The interaction of a water proton with a cage ^{13}C nucleus is therefore expected to be about 6 times larger than the interaction between ortho-water protons in neighbouring cages. It is implausible that a nearby ^{13}C in the same cage would *not* induce spin conversion, while a remote ^{1}H in a neighbouring cage *would*. For these reasons we discount the intermolecular nuclear magnetic dipole-dipole interaction as a plausible spin conversion mechanism, in the current case.

At this stage the detailed mechanism of spin-isomer conversion in $H_2O@C_{60}$ is unknown. It is clear that the interaction between two *ortho* neighbours is involved. But which interaction is that? In our opinion, a strong candidate involves the interaction of the *electric* dipole moments of neighbouring H_2O molecules, possibly mediated by cage-cage interactions. The electric dipole moments couple to the molecular angular momenta in the $J = 1$ states, which are in turn coupled to the nuclear spins through the spin-rotation mechanism—which is already known as a route to unimolecular spin conversion for water in high rotational states.[65,66] The mechanism postulated here would extend the spin-rotation mechanism to bimolecular processes in a low-temperature solid. The rapid increase in the spin conversion rates above 10 K (Table I) could be associated with an increased population of higher rotational levels, which have larger spin-rotation interactions.

Further experiments are needed to elucidate the spin-conversion mechanism. We plan to study the effect of diluting $H_2O@C_{60}$ cages in unfilled C_{60} cages, and the effect of other molecular species and ortho-para spin diffusion on the spin conversion process.

Note added in proof: Sami Jannin (EPFL, Switzerland) has pointed out correctly that the presence of *ortho-para* spin exchange (Eq. (8)) weakens the case for ^{13}C nuclei playing no significant role in the spin conversion process.

ACKNOWLEDGMENTS

The authors acknowledge the support of EPSRC-UK, the National Science Foundation, and the European Research Council. The authors at Columbia thank the National Science Foundation for its support through Grant No. CHE 11-11392. We thank Yasujiro Murata for advice and discussions.

[1] A. Farkas, *Orthohydrogen, Parahydrogen and Heavy Hydrogen* (Cambdrige University Press, 1935), p. 216.
[2] P. Bunker and P. Jensen, *Molecular Symmetry and Spectroscopy*, 2nd ed. (NRC Research Press, Ottawa, 1998), p. 752.
[3] M. J. Mumma, H. A. Weaver, and H. P. Larson, Astron. Astropyphys. **187**, 419 (1987).
[4] J. Crovisier, Science **275**, 1904 (1997).
[5] D. C. Lis, T. G. Phillips, P. F. Goldsmith, D. A. Neufeld, E. Herbst, C. Comito, P. Schilke, H. S. P. Müller, E. A. Bergin, M. Gerin, T. A. Bell, M. Emprechtinger, J. H. Black, G. A. Blake, F. Boulanger, E. Caux, C. Ceccarelli, J. Cernicharo, A. Coutens, N. R. Crockett, F. Daniel, E. Dartois, M. De Luca, M.-L. Dubernet, P. Encrenaz, E. Falgarone, T. R. Geballe, B. Godard, T. F. Giesen, J. R. Goicoechea, C. Gry, H. Gupta, P. Hennebelle, P. Hily-Blant, R. Kołos, J. Krełowski, C. Joblin, D. Johnstone, M. Kaźmierczak, S. D. Lord, S. Maret, P. G. Martin, J. Martín-Pintado, G. J. Melnick, K. M. Menten, R. Monje, B. Mookerjea, P. Morris, J. A. Murphy, V. Ossenkopf, J. C. Pearson, M. Pérault, C. Persson, R. Plume, S.-L. Qin, M. Salez, S. Schlemmer, M. Schmidt, P. Sonnentrucker, J. Stutzki, D. Teyssier, N. Trappe, F. F. S. van der Tak, C. Vastel, S. Wang, H. W. Yorke, S. Yu, J. Zmuidzinas, A. Boogert, N. Erickson, A. Karpov, J. Kooi, F. W. Maiwald, R. Schieder, and P. Zaal, Astron. Astropyphys. **521**, L26 (2010).
[6] M. Emprechtinger, D. C. Lis, T. Bell, T. G. Phillips, P. Schilke, C. Comito, R. Rolffs, F. van der Tak, C. Ceccarelli, H. Aarts, A. Bacmann, A. Baudry, M. Benedettini, E. A. Bergin, G. Blake, A. Boogert, S. Bottinelli, S. Cabrit,

P. Caselli, A. Castets, E. Caux, J. Cernicharo, C. Codella, A. Coutens, N. Crimier, K. Demyk, C. Dominik, P. Encrenaz, E. Falgarone, A. Fuente, M. Gerin, P. Goldsmith, F. Helmich, P. Hennebelle, T. Henning, E. Herbst, P. Hily-Blant, T. Jacq, C. Kahane, M. Kama, A. Klotz, J. Kooi, W. Langer, B. Lefloch, A. Loose, S. Lord, A. Lorenzani, S. Maret, G. Melnick, D. Neufeld, B. Nisini, V. Ossenkopf, S. Pacheco, L. Pagani, B. Parise, J. Pearson, C. Risacher, M. Salez, P. Saraceno, K. Schuster, J. Stutzki, X. Tielens, M. van der Wiel, C. Vastel, S. Viti, V. Wakelam, A. Walters, F. Wyrowski, and H. Yorke, Astron. Astropyphys. **521**, L28 (2010).

[7] T. Kravchuk, M. Reznikov, P. Tichonov, N. Avidor, Y. Meir, A. Bekkerman, and G. Alexandrowicz, Science **331**, 319 (2011).

[8] V. I. Tikhonov and A. A. Volkov, Science **296**, 2363 (2002).

[9] S. L. Veber, E. G. Bagryanskaya, and P. L. Chapovsky, J. Exp. Theor. Phys. **102**, 76 (2006).

[10] R. L. Redington and D. E. Milligan, J. Chem. Phys. **39**, 1276 (1963).

[11] M. E. Fajardo, S. Tam, and M. E. DeRose, J. Mol. Struct. **695–696**, 111 (2004).

[12] R. Sliter, M. Gish, and A. F. Vilesov, J. Phys. Chem. A **115**, 9682 (2011).

[13] J. Tennyson, J. Phys. Chem. Ref. Data **30**, 735 (2001).

[14] G. Buntkowsky, H.-H. Limbach, B. Walaszek, A. Adamczyk, Y. Xu, H. Breitzke, A. Schweitzer, T. Gutmann, M. Wächtler, N. Amadeu, D. Tietze, and B. Chaudret, Z. Phys. Chem. **222**, 1049 (2008).

[15] Z.-D. Sun, K. Takagi, and F. Matsushima, Science **310**, 1938 (2005).

[16] V. V. Zhivonitko, K. V. Kovtunov, P. L. Chapovsky, and I. V. Koptyug, Angew. Chem., Int. Ed. **52**, 13251 (2013).

[17] P. L. Chapovsky, V. V. Zhivonitko, and I. V. Koptyug, J. Phys. Chem. A **117**, 9673 (2013).

[18] K. Tomita, Phys. Rev. **89**, 429 (1953).

[19] M. Miki and T. Momose, Low Temp. Phys. **26**, 661 (2000).

[20] Y. Miyamoto, M. Fushitani, D. Ando, and T. Momose, J. Chem. Phys. **128**, 114502 (2008).

[21] Y. Ji, J. A. Hamida, and N. S. Sullivan, J. Low Temp. Phys. **158**, 509 (2009).

[22] J. Haupt, Phys. Lett. A **38**, 389 (1972).

[23] A. Horsewill, Prog. Nucl. Magn. Reson. Spectrosc. **35**, 359 (1999).

[24] M. Icker and S. Berger, J. Magn. Reson. **219**, 1 (2012).

[25] B. Meier, J.-N. Dumez, G. Stevanato, J. T. Hill-Cousins, S. S. Roy, P. Håkansson, S. Mamone, R. C. D. Brown, G. Pileio, and M. H. Levitt, J. Am. Chem. Soc. **135**, 18746 (2013).

[26] C. R. Bowers and D. P. Weitekamp, Phys. Rev. Lett. **57**, 2645 (1986).

[27] C. R. Bowers and D. P. Weitekamp, J. Am. Chem. Soc. **109**, 5541 (1987).

[28] T. C. Eisenschmid, R. U. Kirss, P. P. Deutsch, S. I. Hommeltoft, R. Eisenberg, J. Bargon, R. G. Lawler, and A. L. Balch, J. Am. Chem. Soc. **109**, 8089 (1987).

[29] M. G. Pravica and D. P. Weitekamp, Chem. Phys. Lett. **145**, 255 (1988).

[30] J. Natterer and J. Bargon, Prog. Nucl. Magn. Reson. Spectrosc. **31**, 293 (1997).

[31] M. Carravetta, O. Johannessen, and M. Levitt, Phys. Rev. Lett. **92**, 153003 (2004).

[32] M. Carravetta and M. H. Levitt, J. Am. Chem. Soc. **126**, 6228 (2004).

[33] M. Carravetta and M. H. Levitt, J. Chem. Phys. **122**, 214505 (2005).

[34] S. Cavadini, J. Dittmer, S. Antonijevic, and G. Bodenhausen, J. Am. Chem. Soc. **127**, 15744 (2005).

[35] R. Sarkar, P. R. Vasos, and G. Bodenhausen, J. Am. Chem. Soc. **129**, 328 (2007).

[36] M. H. Levitt, Annu. Rev. Phys. Chem. **63**, 89 (2012).

[37] W. S. Warren, E. Jenista, R. T. Branca, and X. Chen, Science **323**, 1711 (2009).

[38] P. R. Vasos, A. Comment, R. Sarkar, P. Ahuja, S. Jannin, J.-P. Ansermet, J. A. Konter, P. Hautle, B. van den Brandt, and G. Bodenhausen, Proc. Natl. Acad. Sci. U.S.A. **106**, 18469 (2009).

[39] S. J. Devience, R. L. Walsworth, and M. S. Rosen, NMR Biomed. **26**, 1204 (2013).

[40] K. Kurotobi and Y. Murata, Science **333**, 613 (2011).

[41] A. Krachmalnicoff, M. H. Levitt, and R. J. Whitby, "An optimised scalable synthesis of $H_2O@C_{60}$ and a new synthesis of $H_2@C_{60}$" (unpublished).

[42] C. Beduz, M. Carravetta, J. Y.-C. Chen, M. Concistrè, M. Denning, M. Frunzi, A. J. Horsewill, O. G. Johannessen, R. Lawler, X. Lei, M. H. Levitt, Y. Li, S. Mamone, Y. Murata, U. Nagel, T. Nishida, J. Ollivier, S. Rols, T. Rõõm, R. Sarkar, N. J. Turro, and Y. Yang, Proc. Natl. Acad. Sci. U.S.A. **109**, 12894 (2012).

[43] L. Abouaf-Marguin, A.-M. Vasserot, C. Pardanaud, and X. Michaut, Chem. Phys. Lett. **480**, 82 (2009).

[44] M. Hiller, E. V. Lavrov, and J. Weber, Phys. Rev. Lett. **98**, 055504 (2007).

[45] M. Concistrè, S. Mamone, M. Denning, G. Pileio, X. Lei, Y. Li, M. Carravetta, N. J. Turro, and M. H. Levitt, Philos. Trans. R. Soc. A **371**, 20120102 (2013).

[46] K. Motizuki and T. Nagamiya, J. Phys. Soc. Jpn. **11**, 93 (1956).

[47] F. Schmidt, Phys. Rev. B **10**, 4480 (1974).

[48] I. Silvera, Rev. Mod. Phys. **52**, 393 (1980).

[49] A. Driessen, E. van der Poll, and I. Silvera, Phys. Rev. B **30**, 2517 (1984).

[50] S. Hartmann and E. Hahn, Phys. Rev. **128**, 2042 (1962).

[51] A. Pines, J. Chem. Phys. **59**, 569 (1973).

[52] R. Tycko, R. C. Haddon, G. Dabbagh, S. H. Glarum, D. C. Douglass, and A. M. Mujsce, J. Phys. Chem. **95**, 518 (1991).

[53] M. Carravetta, A. Danquigny, S. Mamone, F. Cuda, O. G. Johannessen, I. Heinmaa, K. Panesar, R. Stern, M. C. Grossel, A. J. Horsewill, A. Samoson, M. Murata, Y. Murata, K. Komatsu, and M. H. Levitt, Phys. Chem. Chem. Phys. **9**, 4879 (2007).

[54] M. Levitt, *Spin Dynamics. Basics of Nuclear Magnetic Resonance*, 2nd ed. (John Wiley and Sons, Chichester, 2008), p. 744.

[55] P. W. Fowler, P. Lazzeretti, M. Malagoli, and R. Zanasi, J. Phys. Chem. **95**, 6404 (1991).

[56] K. Komatsu, M. Murata, and Y. Murata, Science **307**, 238 (2005).

[57] R. Sarkar, M. Concistrè, O. G. Johannessen, P. Beckett, M. Denning, M. Carravetta, M. Al-Mosawi, C. Beduz, Y. Yang, and M. H. Levitt, J. Magn. Reson. **212**, 460 (2011).

[58] J. Sethnna, *Statistical Mechanics: Entropy, Order Parameters and Complexity* (Oxford University Press, Oxford, 2006), p. 376.

[59] W. I. F. David, R. M. Ibberson, T. J. S. Dennis, J. P. Hare, and K. Prassides, Europhys. Lett. **18**, 219 (1992).

[60] M. S. Dresselhaus, G. Dresselhaus, and P. C. Eklund, *Science of Fullerenes and Carbon Nanotubes* (Academic Press, San Diego, 1996), p. 965.

[61] R. Oyarzun and J. Van Kranendonk, Can. J. Phys. **50**, 1494 (1972).

[62] J. Van Kranendonk, *Solid Hydrogen: Theory and Properties of Solid H_2, HD and D_2* (Springer, 1983).

[63] A. J. Horsewill and C. Sun, J. Magn. Reson. **199**, 10 (2009).

[64] A. Berlinsky and W. Hardy, Phys. Rev. B **8**, 5013 (1973).

[65] R. F. Curl, J. Chem. Phys. **46**, 3220 (1967).

[66] P. Cacciani, J. Cosléou, and M. Khelkhal, Phys. Rev. A **85**, 012521 (2012).